Plasmonic Effects on the Growth of Ag Nanocrystals in Solution

E. Sutter[1,*] M. Sun,[1] Y. Li,[2] B. Zhang,[1] C. Argyropoulos,[2] and P. Sutter[2]

[1]*Department of Mechanical and Materials Engineering, University of Nebraska-Lincoln, Lincoln, NE 68588 (USA)*

[2]*Department of Electrical and Computer Engineering, University of Nebraska-Lincoln, Lincoln, NE 68588 (USA)*

ABSTRACT

The light-stimulated transformation of ensembles of spherical nanoparticles into anisotropic metal nanostructures mediated by localized surface plasmon resonance (LSPR) excitation is an elegant way of synthesizing triangular silver nanoprisms with extraordinary control over size and shape. Generally, the transformation occurs in oxidizing environments along a pathway that involves the oxidative etching of small preexisting Ag seeds, followed by plasmon-mediated reduction of the resulting Ag ions and Ag^0 incorporation into the anisotropic nanocrystals. Here, we investigate pathways toward Ag nanoprisms from initially homogeneous $AgNO_3$ solutions held under reducing conditions. Observations using in situ electron microscopy show that reducing environments and high Ag precursor concentrations in the presence of sodium citrate favor two alternative transformation routes of initial spherical nuclei into anisotropic nanoprisms: (i) the aggregation of spherical nanoparticles and plasmon-mediated conversion of small clusters into triangular prisms; (ii) shape fluctuations of individual small nanoparticles. Simulated field distributions confirm that the coupling of the LSPR excitation between closely spaced nanoparticles causes significant field enhancements near the local plasmonic hot spots, which facilitates accelerated Ag incorporation and thus supports the transformation into nanoprisms.

*Corresponding author: esutter@unl.edu

1. INTRODUCTION

Anisotropic Ag nanocrystals such as triangular prisms have attracted a lot of interest as these two-dimensional plasmonic nanostructures have strongly size-, shape-dependent and thus highly tunable optical properties, localized surface plasmon resonances (LSPRss) and electromagnetic field enhancements, which make them particularly suitable for various nanophotonic devices with applications in photovoltaics,[1] plasmon nanolasers,[2] electrocatalysis,[3] and biomedicine. In addition, citrate stabilized Ag nanoprisms can be functionalized easily using thiol based surface chemistry, an important requirement for biosensing applications using LSPRs and surface enhanced Raman scattering (SERS).[4-5] In solutions-based approaches, Ag nanoprisms can be produced in an elegant and reliable process of photochemical conversion of Ag nanoparticles[6] and chemical synthesis involving reducing agents such as sodium borohydride,[7-8] variety of capping agents, among which sodium citrate plays a special role and hydrogen peroxide (H_2O_2)[9-10] as an etchant with high efficiency and yield. These seeded growth reduction approaches require the initial presence of Ag nanoparticles in the solution either as preformed seeds or as the product of the synthesis first step. It is important to note that visible light is critical for the Ag nanoprism formation, i.e. the growth of anisotropic nanostructures is mediated by excitation of a localized surface plasmon resonance (LSPR) – either directly by driving the photochemical conversion via laser light irradiation[6] or as ambient light affecting the chemical reactions, which importantly do not lead to formation of anisotropic Ag nanoprisms in the dark.[11] Previous work suggests that even in Ag ion containing solutions, i.e. without small Ag seed particles, the formation of the anisotropic Ag nanoprisms proceeds via initial growth of seeds that transform into

prisms.[6, 12] Indeed we recently followed the transformation *in-situ* using liquid cell electron microscopy (LCEM) in solutions containing seed particles on a single particle level.[13] These real time observations clearly demonstrated the oxidation of sparse Ag seeds, the early stages of uniform Ag^0 incorporation in the prism side facets and a further transition to a size regime in which differences in attachment rate could be correlated with local plasmonic field enhancements, which resulted in an experimental determination of the range over which charge carriers transferred from plasmonic hot spots can drive chemistry. However, it remains unclear if direct supply of metal ions would not result into immediate nucleation of the anisotropic nanostructures. Oxidative conditions have been shown to favor the formation of nanoprisms, however, reducing environments with high concentration of silver precursor might offer additional pathways for nucleation of anisotropic structures or transformation of seeds into anisotropic nanoprisms to the one observed in solutions with Ag seeds. To address these questions, we carry out in-situ LCEM observations in aqueous solution containing Ag precursor with and without sodium citrate. We explore a growth regime in which we obtain a high concentration of the silver ions via rapid reduction of the precursor and initial growth of Ag nanoparticles in aqueous solutions containing $AgNO_3$. We investigate the role of sodium citrate, comparing the formation of Ag nanoparticles in solutions with and without sodium citrate. The in-situ observations together with calculations establish that at highly reducing conditions and high concentration of nanoparticles their LSPR-mediated interactions an additional pathway for the formation of nanoprisms along with the direct transformation observed previously.

2. RESULTS AND DISCUSSION

Ag NANOCRYSTALS FORMATION WITHOUT ELECTRON IRRADIATION

To study growth of Ag nanocrystals in solution we performed complementary experiments comprising real-time in-situ liquid cell transmission electron microscopy (TEM) and scanning TEM (STEM), as well as control experiments in which reactions were set to proceed on the bench without electron irradiation. In both cases, ex-situ electron microscopy and complementary analytical methods were used to evaluate the reaction products. We compare the growth of Ag nanocrystals in $AgNO_3$ solution with added sodium citrate (Figure 1, vial 1) and without sodium citrate (Figure 1, vial 2). These solutions were exposed to light for several hours, while identical solutions were kept in the dark (Figure 1, vial 3). The experiments were performed at room temperature without addition of additional reducing agents to ensure conditions identical to those in the microscope. After ~ 1 hour of light exposure the mixed solution turned yellow, at which time UV-VIS spectra of all solutions were measured, an aliquot of the yellow solution was taken out, deposited on a carbon film and investigated by TEM. The UV-VIS spectrum of the yellow solution (Figure 1 (a) – curve 1) shows a large peak centered around 415 nm, which is consistent with the presence of Ag nanocrystals (Ag nanoparticles of ~ 40 nm diameter). The solution without sodium citrate as well as the one with sodium citrate but kept in the dark did not show any changes in color and their UV-VIS spectra remained unchanged (Figure 1 (a) – curve 2,3) even after several hours. Imaging of the nanocrystals formed in the mixed sodium citrate-$AgNO_3$ solution exposed to light showed the development of characteristic anisotropic Ag nanostructures (triangles, rods, hexagons, cubes) together with a large amount of small Ag nanoparticles. The ex-

situ experiments demonstrate that the formation of nanoparticles as well as nanoprisms and other anisotropic nanostructures requires the presence of citrate in the $AgNO_3$ solution in combination with light excitation.

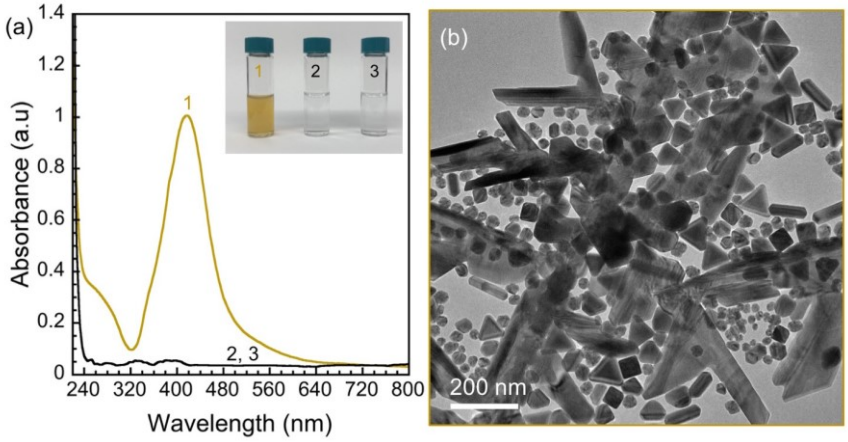

Figure 1. Ag nanostructures growth in an aqueous $AgNO_3$ solution with added sodium citrate. (a) UV-VIS spectra of the aqueous $AgNO_3$ solutions with sodium citrate (yellow curve) and without sodium citrate (black curve), respectively, following exposure to sunlight for 1 h. The three solutions are shown in the inset: Vial 1 - $AgNO_3$ solution (0.35 mM) containing sodium citrate (0.7 mM) exposed to light for 1 h; vial 2 - pure $AgNO_3$ solution (0.35 mM) exposed to light for 1 h; vial 3 - $AgNO_3$ solution (0.35 mM) containing sodium citrate (0.7 mM) kept in the dark for 1 h. **(b)** TEM image of the ensemble of Ag nanostructures with different anisotropic shapes formed in the sodium citrate-containing $AgNO_3$ solution (Vial 1, UV-VIS spectrum 1).

REAL-TIME TEM IMAGING

The aqueous solutions containing either $AgNO_3$ or mixed $AgNO_3$ - sodium citrate, identical to those used in our benchtop reference experiments, were loaded into the liquid cell and subjected to in-situ STEM observations of the Ag nanocrystal formation process. Figure 2 shows a time-lapse series of HAADF-STEM images from Movie S1 which follows the evolution of the aqueous solution containing 350 μM $AgNO_3$. The in-situ LCEM observations of mixed $AgNO_3$ (350 μM) and sodium citrate (700 μM) aqueous solutions (Movie S2) are shown in Figure 3.

Time-lapse HAADF-STEM imaging shows an initially homogeneous and uniform solution (Figure 2 (a)), in which nanoparticles with brighter contrast nucleate and grow

(Figure 2 (b) – (o)). Even a brief exposure of a few seconds of the solution to the electron beam results in the nucleation of nanoparticles; further exposure leads to an increase in their sizes. In parts of the liquid cell outside the field of view (FOV), which have not previously been exposed to electrons, the solution remains free of nanoparticles, but observation by STEM triggers the same nucleation and growth process as described above. Thus, we conclude that i) direct electron irradiation causes radiolysis of water and formation of a cascade of radicals and aqueous electrons (e_{aq}^-). e_{aq}^-, having a standard electrode potential of 2.67 V,[14] can reduce Ag ions into metallic Ag ($Ag^+ + e_{aq}^- \rightarrow Ag^0$) while remote areas of the solution remain unaffected; and ii) the resulting supersaturation of Ag^0 causes Ag nanoparticle nucleation and growth in the solution, which can be readily imaged in real time by STEM similar to earlier in-situ investigations.[15-16]

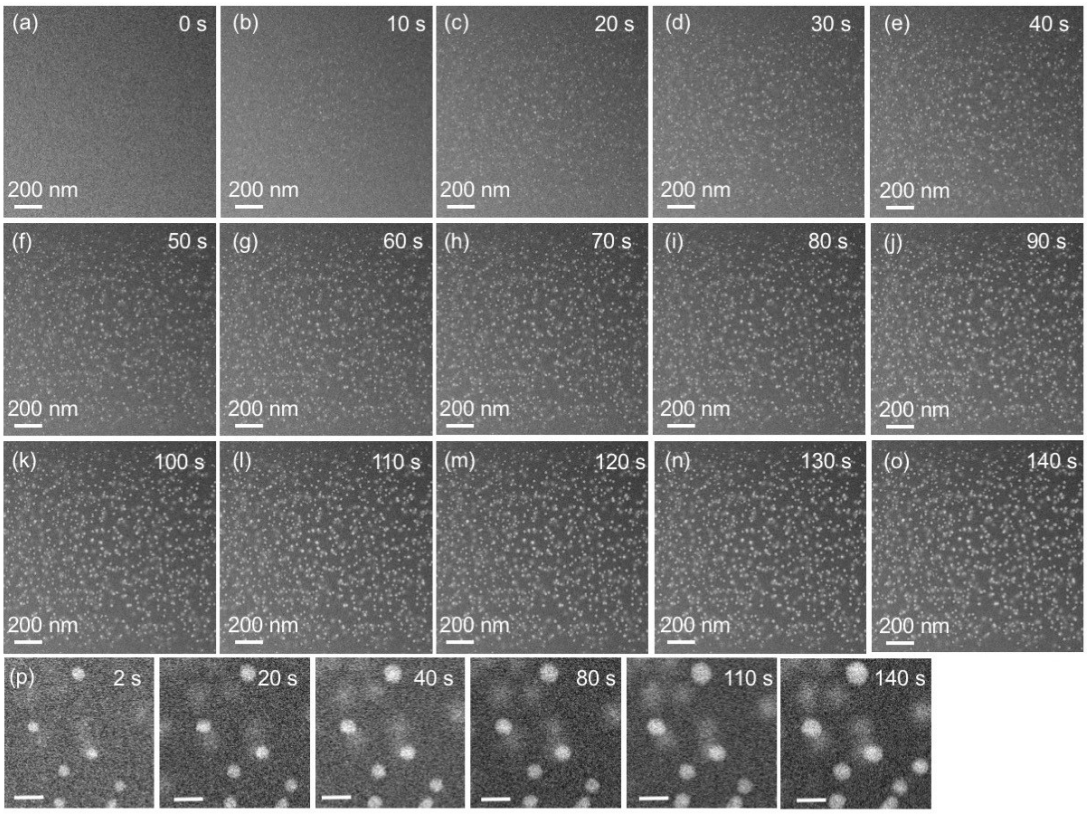

Figure 2. Ag nanoparticles growth in an aqueous $AgNO_3$ solution. (a)-(o) Time-lapse HAADF-STEM images from an *in-situ* electron microscopy movie following the growth of Ag

nanoparticles in aqueous $AgNO_3$ solution (0.35 mM) over 140 s. The elapsed time after the initial exposure to the electron beam is indicated in each image. **(p)** Higher magnification images showing the Ag nanoparticles at different times during observations. Scale bars: 50 nm.

Higher magnification images (Figure 2 (p)) demonstrates clearly that the Ag nanoparticles formed in this process are spherical in shape similar to the nanoparticles of other noble metals such as Pd,[17-18] Au[18] grown in metal salt-containing aqueous solutions. Importantly, during the entire time of observation the Ag nanoparticles remained spherical, i.e. no Ag nanocrystals with anisotropic shapes were found in the absence of sodium citrate.

Introduction of sodium citrate in the $AgNO_3$ aqueous solution leads to significant changes in the growth of Ag nanostructures. Figure 3 (a) shows the solution after a very brief exposure to the electron beam (3 s). Already at this early stage we can see isolated small spherical nanoparticles that are brighter in contrast than the uniform darker background of the solution (similar to Figure 2), confirming that nucleation starts immediately after the exposure to the electron beam in this case as well. Within the first 10 s (Figure 3 (b)) the number of nanoparticles in the field of view increased significantly via fast nucleation of new nanoparticles, while the already formed nanoparticles continue to grow. In comparison to the pure $AgNO_3$ solution, the nucleation appears to last longer in the presence of sodium citrate, most probably due to the fact that sodium can act as a strong complexing stabilizer forming relatively stable complexes with positively charged Ag^+ which are then release gradually as Ag^+ is consumed.[19] Movie S2 and Figure 3 show that the nanocrystals are mobile in the solution, move readily in the field of view and occasionally form short chains and small clusters consisting of a few nanocrystals. A

large number of the Ag nanocrystals remain sufficiently long in the field of view to allow us to follow their growth and interactions over a longer period of time.[18, 20]

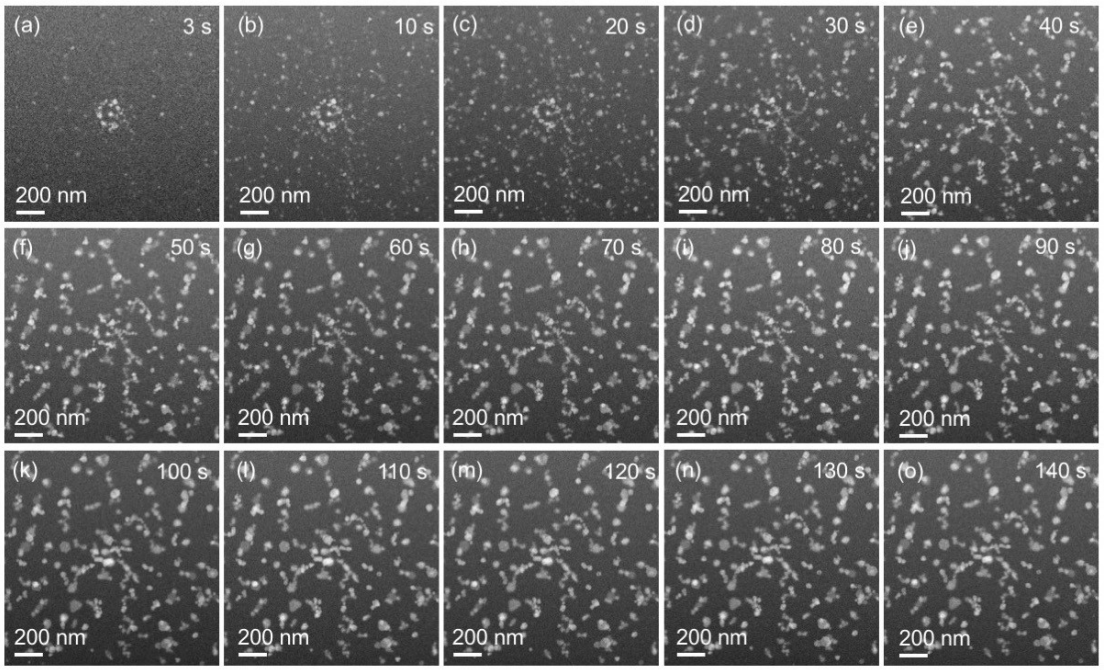

Figure 3. Plasmon-mediated growth of anisotropic Ag nanocrystals. Time-lapse HAADF-STEM images from an *in-situ* electron microscopy movie following the growth of anisotropic Ag nanocrystals in aqueous $AgNO_3$ solution (0.35 mM) with sodium citrate (0.7 mM) over 180 s. The elapsed time after the initial exposure to the electron beam is indicated in each image.

Importantly, in the present experiments a change in the number of nanocrystals due to dissolution is not observed. This is distinctly different from recent experiments that imaged in real time the transformation of Ag nanoparticle seeds into triangular prisms using LCEM, in which the Ag nanoparticles decreased in size, followed by a transformation to Ag nanoplates.[13] Here we establish an overall reducing environment which favors the growth and interaction of the nanocrystals. Shortly after nucleation the nanocrystals in the solution look very different from the uniform spherical nanoparticles that form in the $AgNO_3$ solutions without added sodium citrate (Figure 2), i.e. we see

formation of nanoprisms with different shapes and sizes, in addition to spherical nanoparticles. After electron beam irradiation for 140 s of the mixed $AgNO_3$ – sodium citrate solution, and we find that ~20% of the nanocrystals are Ag nanoprisms and the size of the remaining Ag nanoparticles (Figure 3) are larger than the nanoparticles in Figure 2 even though all experimental conditions are identical. These two main differences, i.e. formation of anisotropic nanoprisms and the larger size of nanocrystals overall, are related to the addition of sodium citrate to the $AgNO_3$ solutions, confirming its important role, similar to the ex-situ experiment, in which sodium citrate was necessary for nanocrystal growth (Figure 1, vial 1). Wet-chemistry synthesis of Ag nanocrystals, invariably results in formation of spherical Ag nanoparticles in the dark,[21-22] thus ruling out the possibility that citrate acts as a ligand promoting anisotropic character in nanostructures similar to PVP[27, 28]. Citrate is indeed well established as the hole scavenger needed in complex photochemical processes that involve plasmon-mediated growth of anisotropic Ag nanoprisms via Landau damping of the hot electron-hole pair.[21, 23-25] Briefly, in the process of Ag nanoparticle-to-nanoprism conversion oxidative etching dissolves small Ag nanoparticles to provide Ag^+ ions in solution.[26-27] The reduction of Ag^+ to Ag^0, the primary plasmon-mediated process, is believed to involve Landau damping of the LSPR to produce hot electron-hole pairs.[28] A hole scavenger, i.e. the particle-bound sodium citrate, is irreversibly oxidized and desorbs from the particle.[29] The residual net charge (2 e^- per citrate) can reduce Ag^+ ions on the nanoparticle surface to Ag^0, which results in Ag growth exclusively on the side facet.[6, 30] High-energy electrons used for imaging excite LSPRs in the nanoparticles.[13, 31-32] The propagating electron represent a localized (down to spot sizes below 1 nm) evanescent source of

supercontinuum light that provides an optical excitation analogous to conventional broadband light sources (Figure 4). Thus, the electron-induced local electromagnetic excitations due to the scanned STEM probe excite LSPRs in Ag nanostructures and the addition of sodium citrate (Figure 3) allows the hot hole from the electron-hole pair to be removed and the hot electron to participate in the growth. This effect modifies the straight forward nucleation and growth of nanoparticles observed in the absence of sodium citrate (Figure 2) and introduces a plasmon-mediated enhancement in the growth of Ag nanostructures.

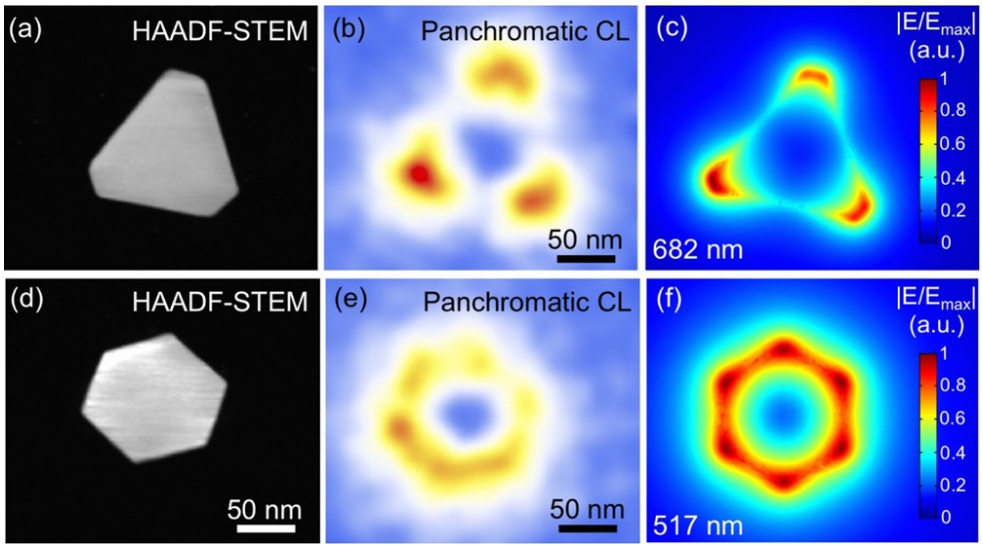

Figure 4. Evidence for the excitation of localized surface plasmon resonances in anisotropic Ag nanocrystals by the focused electron beam in STEM. (a) HAADF-STEM image, **(b)** corresponding panchromatic STEM-cathodoluminescence (STEM-CL) map of a truncated Ag nanoprism, showing strong luminescence from the corners. The coupling of the electron beam to the LSPR is strongest at the corners of the Ag prism. **(c)** Simulated field distribution of the dipolar plasmon resonance mode for the Ag nanoprism in (a). Substrate: SiO_2 (n = 1.47). **(d)** HAADF-STEM image, **(e)** corresponding panchromatic STEM-CL map of a hexagonal Ag nanoprism, showing strong luminescence from corners and edges. **(f)** Simulated field distribution of the dipolar plasmon resonance mode for the hexagonal Ag nanoprism. Substrate: SiO_2 (n = 1.47).

The in-situ LCEM observations demonstrate two pathways to anisotropic Ag nanostructures in the mixed $AgNO_3$ – sodium citrate aqueous solution: (i) interaction of

closely spaced spherical nanoparticles (Figure 5) and (ii) shape fluctuations of small nanoparticles (Figure 7). The time-lapse sequence of *in-situ* HAADF-STEM images in Figure 5 (zoomed-in from Fig. 3) highlights the evolution of a cluster of closely spaced Ag nanoparticles with time and its transformation to a truncated triangular nanoplate. During the initial 19 s three spherical Ag nanoparticles come close together and form a cluster. This cluster surprisingly does not coalesce but is seen to add material in particular directions (22 s), change overall shape and become gradually more anisotropic until it is replaced by a single truncated triangular plate (24 s). This process is distinctly different from coalescence of closely spaced nanoparticles[33-34] which never yields well-defined shapes.

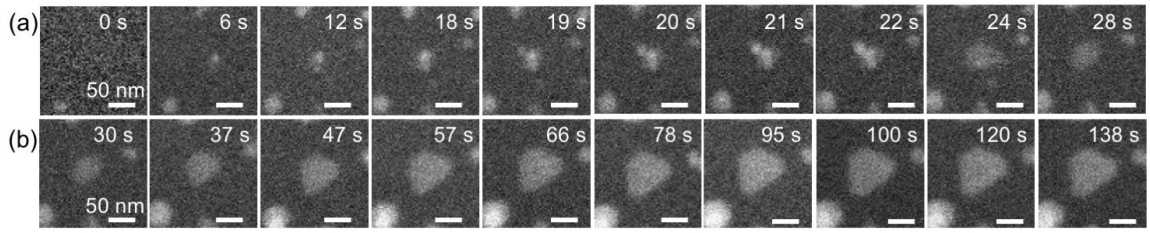

Figure 5. *In-situ* liquid cell electron microscopy of plasmon-mediated Ag nanoprism growth in mixed solutions of $AgNO_3$ and sodium citrate. (a) Time-lapse sequence of *in-situ* HAADF-STEM images (zoomed-in from Fig. 3) showing the formation of a small plate-like Ag nanocrystal through interaction of small Ag nanoparticles during the initial growth stage (t = 0 s to 28 s). **(b)** Following the formation of this anisotropic nucleus from closely-spaced spherical particles, the plate grows shape-invariant as a truncated Ag nanoprism.

The observed interaction of the cluster of nanoparticles is mediated by the LSPRs of the individual Ag nanoparticles excited by the moving electron probe.[13] When the nanoparticles are in a cluster strong coupling can occur that leads to rearrangement of field distribution and local field enhancements (hot spots).[35-36] We performed simulations of the field distribution around a cluster of three Ag nanoparticles with 20 nm diameter as a function of the position of the moving electron probe (Figure 6 (a)). The extinction

cross-section (ECS) (Figure 6 (b), shows that the dipolar resonance mode (422 nm) dominates but higher order modes (386 nm, 375 nm) are also excited. The field distributions of these modes as a function of the position of the excitation source are shown in Figure 6 (c) – (g). The simulations show strong coupling between the LSPRs of the three particles and strong field enhancements located at the gaps between the nanoparticles for all positions and at the periphery of the cluster (Figure 6 (e)). The significant field enhancement, particularly in the area between particles, promotes enhanced reduction of Ag precursor by electrons supplied by Landau damping of the LSPR and local incorporation of Ag^0 into the active parts of the surface in a plasmon-mediated growth process. Thus, the nanocrystal growth is accelerated locally at the areas corresponding to the hot spots, as a result of which the group of nanoparticles morphs into a truncated triangular prism, as observed by *in-situ* LCEM sequence (Figure 5 (a)). After the formation of the prism the field distribution changes significantly (Figure 4 (a)-(c)). For small triangular nanoprisms (Figure 4 (a)), cathodoluminescence (CL) maps using the excitation by the scanning electron probe and far-field detection of the emitted light (Figure 4 (b)) as well as simulations (Figure 4 (c)) show strongest coupling to the LSPR when the electron probe resides near the corners of Ag nanoprisms and at this stage the plasmon-mediated growth of the triangular Ag prism proceeds continuously to ~ 100 nm size, similar to earlier observations.[13]

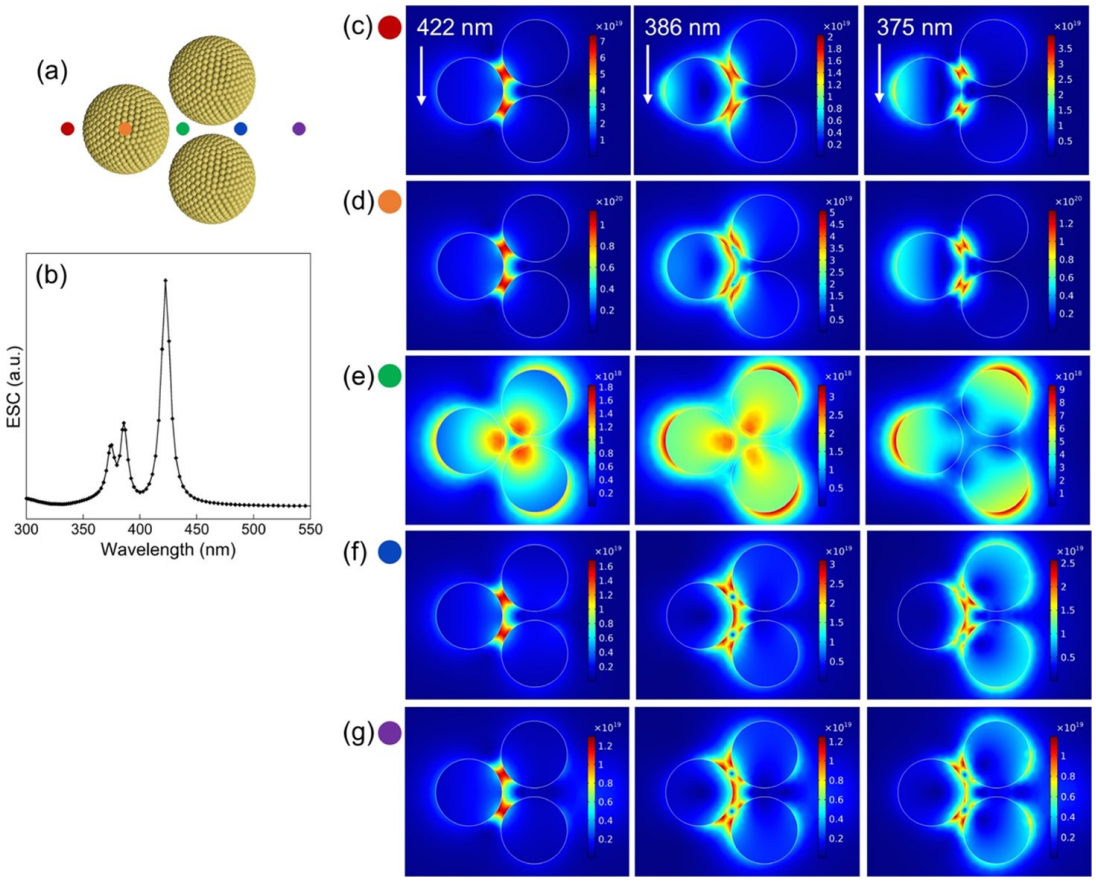

Figure 6. Simulated field distribution for a cluster of three Ag nanoparticles. (a) Schematic showing a group of three particles (diameter: 20 nm, interparticle distance: 2 nm) used in the calculation of the extinction cross-section (ECS) shown in (b). The calculation uses a point dipole light source to model the localized electromagnetic excitation by the field of the focused electron beam. **(b)** Calculated ECS of the trimer nanostructure in (a). **(c)-(g)** Field distributions of the dipole- (λ = 422 nm) and higher-order (λ = 386 nm, 375 nm) plasmon resonances calculated for the different point dipole positions designated by colored dots in (a).

A second pathway to anisotropic nanostructures involves the presence of anisotropy possibly by shape fluctuation in the initial stages of growth of a Ag nanoparticle. Figure 7 follows the formation of a hexagonal prism via this route. Almost immediately after irradiation with the electron beam and nucleation (Figure 7 (5 s)) the nanoparticle shows a deviation from spherical shape and evolves quickly into a hexagonal plate with well-defined edges (Figure 7 (12 s)). Further, the nanoplate preserves its hexagonal shape and clearly increases in size (Figure 7 (12 s – 94 s)). For a small hexagonal nanoprism (Figure 4 (d)), CL maps (Figure 4 (e)) as well as simulations (Figure 4 (f)) show strongest hot

spots distributed along the entire periphery of the Ag nanoprism. The thickness of this plate is estimated from the intensity of the HAADF-STEM images and normalized by the intensity of spherical particles in the same solution[13] to be ~ 20 nm. The real-time observations show that the thickness remains unchanged with time while the edges increase in length. Such behavior is consistent with a plasmon mediated growth process similar to the ones for the triangular prism in Figure 5.

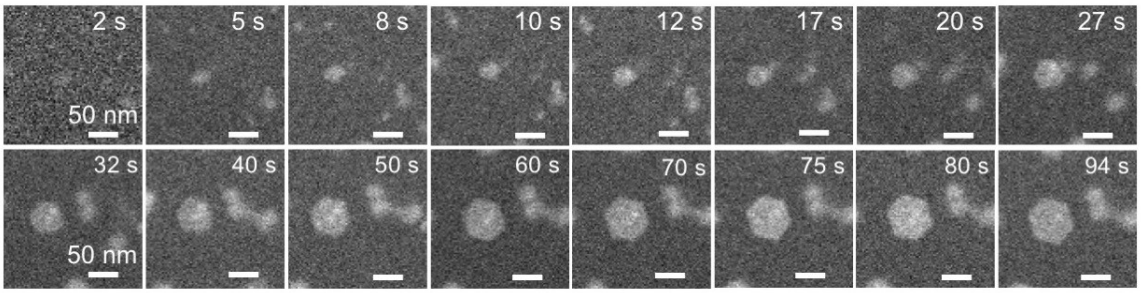

Figure 7. *In-situ* liquid cell electron microscopy of plasmon-mediated Ag nanoprism growth in aqueous $AgNO_3$ solutions with sodium citrate. Time-lapse sequence of in-situ HAADF-STEM images showing the nucleation and growth of a hexagonal Ag nanoprism.

3. CONCLUSIONS

In summary, we carried out in-situ electron microscopy observations of the growth of Ag nanocrystals in silver nitrate solutions with and without sodium citrate. While the growth in pure $AgNO_3$ solutions results in formation of Ag nanoparticles, the addition of sodium citrate leads to the formation of nanoparticles as well as anisotropic nanostructures similar to control experiments without electron irradiation. The in-situ observations establish two distinct pathways for formation of Ag nanoprisms: (i) interactions of nanoparticles and (ii) fluctuations in the shape of small seeds. Simulations substantiate strong LSPR field enhancements as the possible driving force for the transformation of clusters of nanoparticles into nanoprisms.

4. MATERIALS AND METHODS

Silver nitrate ($AgNO_3$) 0.7 mM stock solution was prepared by dissolving $AgNO_3$ salt in deionized (DI) water (Millipore grade: 18.2 MΩ). Two types of solutions were prepared for the ex-situ and in-situ experiments. *(i.)* $AgNO_3$ aqueous solution prepared from the stock $AgNO_3$ solution (0.7 mM) by dilution with DI water to 0.35 mM. *(ii.)* Mixed $AgNO_3$ – $HOC(COONa)(CH_2COONa)_2 \cdot 2H_2O$ (sodium citrate tribasic dihydrate, which we call sodium citrate in the manuscript) aqueous solution, prepared by addition of aqueous solution containing sodium citrate (1.4 mM) to the stock $AgNO_3$ solution (0.7 mM) to obtain a concentration of 0.35 mM $AgNO_3$ and 0.7 mM citrate. Fresh solutions were prepared immediately before each experiment. A microdroplet (~ 0.5 μL) of the mixed solution was then loaded between two 30 nm thick SiN_x membranes supported on Si frames. The LCEM experiments were carried out in a dedicated specimen holder (Hummingbird Scientific). Time-lapse HAADF-STEM (Z-contrast) imaging was performed in a FEI Talos F200X microscope operated at 200 kV with ~2 Å probe size and beam current ~ 16 pA, measured in vacuum before introduction of the liquid cell. For the time-lapsed STEM images in figure 2 and figure 3 (Movies S1 and S2), the acquisition conditions were 512 × 512 pixels, pixel dwell time − 4 μs, 1.05 s/frame, electron dose per image: 14.8 $e^-/Å^2$, electron dose rate: 14.1 $e^-/Å^2 \cdot s$.

Cathodoluminescence (CL) measurements were performed in HAADF-STEM mode (STEM-CL) with local excitation and far-field light collection using a Gatan Vulcan CL holder at room temperature and 200 kV electron energy. The incident beam current for CL measurements was ~ 300 pA. The panchromatic CL maps in figure 6 are 100 × 100 pixels with acquisition time of 100 ms per pixel.

Full-wave simulations of the nanostructures were performed using the commercial finite-element simulation software COMSOL Multiphysics. A spherical domain around a single nanostructure was created and perfectly matched layer absorbing boundary conditions were employed to mimic an open boundary. The Ag nanoparticles in Figure 6 are surrounded by water with refractive index n = 1.33. Realistic permittivity values of Ag as a function of wavelength were used in the simulations based on previously derived experimental data.[37] To obtain the ECS signature of the nanostructures shown in Figure 6(b), the scattered-field formulation was employed, which directly computes the scattered fields by using the analytical solution for an incident plane wave in the absence of the nanostructures as the background field. The incident angle of the excitation wave is normal to the surface. To compute the electric field distributions of the dipole, quadrupole, and higher order modes of the Ag nanostructures shown in Figures 4 and 6, a point-dipole source was introduced at the near-field of the sample to stimulate each mode at the corresponding resonance frequencies.

5. ACKNOWLEDGEMENTS

This material is based upon work supported by the U. S. Army Research Laboratory and the U.S. Army Research Office under grant number W911NF-17-1-0141. The authors acknowledge seed funding from the Nebraska Public Power District through the Nebraska Center for Energy Sciences Research. Y. Li and C. Argyropoulos thank the National Science Foundation (DMR-1709612) and the Nebraska Materials Research Science and Engineering Center (MRSEC) (DMR-1420645) for providing partial support for this work.

REFERENCES:

1. Atwater, H. A.; Polman, A. Plasmonics for Improved Photovoltaic Devices. *Nat Mater* **2010**, *9*, 205.
2. Oulton, R. F.; Sorger, V. J.; Zentgraf, T.; Ma, R.-M.; Gladden, C.; Dai, L.; Bartal, G.; Zhang, X. Plasmon Lasers at Deep Subwavelength Scale. *Nature* **2009**, *461*, 629.
3. Liu, S.; Tao, H.; Zeng, L.; Liu, Q.; Xu, Z.; Liu, Q.; Luo, J.-L. Shape-Dependent Electrocatalytic Reduction of Co2 to Co on Triangular Silver Nanoplates. *J Am Chem Soc* **2017**, *139*, 2160-2163.
4. Haber, J.; Sokolov, K. Synthesis of Stable Citrate-Capped Silver Nanoprisms. *Langmuir* **2017**, *33*, 10525-10530.
5. Kelly, K. L.; Coronado, E.; Zhao, L. L.; Schatz, G. C. The Optical Properties of Metal Nanoparticles: The Influence of Size, Shape, and Dielectric Environment. *The Journal of Physical Chemistry B* **2003**, *107*, 668-677.
6. Jin, R.; Cao, Y.; Mirkin, C. A.; Kelly, K. L.; Schatz, G. C.; Zheng, J. G. Photoinduced Conversion of Silver Nanospheres to Nanoprisms. *Science* **2001**, *294*, 1901-1903.
7. Métraux, G. S.; Mirkin, C. A. Rapid Thermal Synthesis of Silver Nanoprisms with Chemically Tailorable Thickness. *Adv Mater* **2005**, *17*, 412-415.
8. Zhang, Q.; Hu, Y.; Guo, S.; Goebl, J.; Yin, Y. Seeded Growth of Uniform Ag Nanoplates with High Aspect Ratio and Widely Tunable Surface Plasmon Bands. *Nano Lett* **2010**, *10*, 5037-5042.
9. Zhang, Q.; Li, N.; Goebl, J.; Lu, Z.; Yin, Y. A Systematic Study of the Synthesis of Silver Nanoplates: Is Citrate a "Magic" Reagent? *J Am Chem Soc* **2011**, *133*, 18931-18939.
10. Parnklang, T.; Lertvachirapaiboon, C.; Pienpinijtham, P.; Wongravee, K.; Thammacharoen, C.; Ekgasit, S. H2o2-Triggered Shape Transformation of Silver Nanospheres to Nanoprisms with Controllable Longitudinal Lspr Wavelengths. *RSC Advances* **2013**, *3*, 12886-12894.
11. Yu, H.; Zhang, Q.; Liu, H.; Dahl, M.; Joo, J. B.; Li, N.; Wang, L.; Yin, Y. Thermal Synthesis of Silver Nanoplates Revisited: A Modified Photochemical Process. *Acs Nano* **2014**, *8*, 10252-10261.
12. Sun, Y.; Xia, Y. Triangular Nanoplates of Silver: Synthesis, Characterization, and Use as Sacrificial Templates for Generating Triangular Nanorings of Gold. *Adv Mater* **2003**, *15*, 695-699.
13. Sutter, P.; Li, Y.; Argyropoulos, C.; Sutter, E. In Situ Electron Microscopy of Plasmon-Mediated Nanocrystal Synthesis. *J Am Chem Soc* **2017**, *139*, 6771-6776.
14. Walker, D. C. The Hydrated Electron. *Quarterly Reviews, Chemical Society* **1967**, *21*, 79-108.
15. Woehl, T. J.; Park, C.; Evans, J. E.; Arslan, I.; Ristenpart, W. D.; Browning, N. D. Direct Observation of Aggregative Nanoparticle Growth: Kinetic Modeling of the Size Distribution and Growth Rate. *Nano Lett.* **2014**, *14*, 373-378.
16. Loh, N. D.; Sen, S.; Bosman, M.; Tan, S. F.; Zhong, J.; Nijhuis, C. A.; Kral, P.; Matsudaira, P.; Mirsaidov, U. Multistep Nucleation of Nanocrystals in Aqueous Solution. *Nature Chemistry* **2017**, *9*, 77-82.
17. Jungjohann, K. L.; Bliznakov, S.; Sutter, P. W.; Stach, E. A.; Sutter, E. A. In Situ Liquid Cell Electron Microscopy of the Solution Growth of Au-Pd Core-Shell Nanostructures. *Nano Lett* **2013**, *13*, 2964-2970.

18. Sutter, E. A.; Sutter, P. W. Determination of Redox Reaction Rates and Orders by in Situ Liquid Cell Electron Microscopy of Pd and Au Solution Growth. *J Am Chem Soc* **2014**, *136*, 16865-16870.
19. Bastús, N. G.; Merkoçi, F.; Piella, J.; Puntes, V. Synthesis of Highly Monodisperse Citrate-Stabilized Silver Nanoparticles of up to 200 Nm: Kinetic Control and Catalytic Properties. *Chem. Mater.* **2014**, *26*, 2836-2846.
20. Sutter, E. A.; Sutter, P. W. In Situ Liquid Cell Electron Microscopy of Ag-Au Galvanic Replacement Reactions. *Nanoscale* **2017**, *9*, 1271-1278.
21. Jin, R. C.; Cao, Y. W.; Mirkin, C. A.; Kelly, K. L.; Schatz, G. C.; Zheng, J. G. Photoinduced Conversion of Silver Nanospheres to Nanoprisms. *Science* **2001**, *294*, 1901-1903.
22. Maillard, M.; Huang, P.; Brus, L. Silver Nanodisk Growth by Surface Plasmon Enhanced Photoreduction of Adsorbed [Ag+]. *Nano Lett* **2003**, *3*, 1611-1615.
23. Jin, R. C.; Cao, Y. C.; Hao, E. C.; Metraux, G. S.; Schatz, G. C.; Mirkin, C. A. Controlling Anisotropic Nanoparticle Growth through Plasmon Excitation. *Nature* **2003**, *425*, 487-490.
24. Langille, M. R.; Personick, M. L.; Mirkin, C. A. Plasmon-Mediated Syntheses of Metallic Nanostructures. *Angewandte Chemie International Edition* **2013**, *52*, 13910-13940.
25. Zhai, Y.; DuChene, J. S.; Wang, Y.-C.; Qiu, J.; Johnston-Peck, A. C.; You, B.; Guo, W.; DiCiaccio, B.; Qian, K.; Zhao, E. W. Polyvinylpyrrolidone-Induced Anisotropic Growth of Gold Nanoprisms in Plasmon-Driven Synthesis. *Nature materials* **2016**, *15*, 889.
26. Xue, C.; Métraux, G. S.; Millstone, J. E.; Mirkin, C. A. Mechanistic Study of Photomediated Triangular Silver Nanoprism Growth. *J Am Chem Soc* **2008**, *130*, 8337-8344.
27. Wu, X.; Redmond, P. L.; Liu, H.; Chen, Y.; Steigerwald, M.; Brus, L. Photovoltage Mechanism for Room Light Conversion of Citrate Stabilized Silver Nanocrystal Seeds to Large Nanoprisms. *J Am Chem Soc* **2008**, *130*, 9500-9506.
28. Govorov, A. O.; Zhang, H.; Demir, H. V.; Gun'ko, Y. K. Photogeneration of Hot Plasmonic Electrons with Metal Nanocrystals: Quantum Description and Potential Applications. *Nano Today* **2014**, *9*, 85-101.
29. Redmond, P. L.; Wu, X.; Brus, L. Photovoltage and Photocatalyzed Growth in Citrate-Stabilized Colloidal Silver Nanocrystals. *J Phys Chem C* **2007**, *111*, 8942-8947.
30. Jin, R.; Cao, C. Y.; Hao, E.; Metraux, G. S.; Schatz, G. C.; Mirkin, C. A. Controlling Anisotropic Nanoparticle Growth through Plasmon Excitation. *Nature* **2003**, *425*, 487-490.
31. García de Abajo, F. J. Optical Excitations in Electron Microscopy. *Reviews of Modern Physics* **2010**, *82*, 209-275.
32. Kociak, M.; Stéphan, O.; Gloter, A.; Zagonel, L. F.; Tizei, L. H. G.; Tencé, M.; March, K.; Blazit, J. D.; Mahfoud, Z.; Losquin, A.; Meuret, S.; Colliex, C. Seeing and Measuring in Colours: Electron Microscopy and Spectroscopies Applied to Nano-Optics. *Comptes Rendus Physique* **2014**, *15*, 158-175.
33. Sutter, E.; Sutter, P.; Zhu, Y. Assembly and Interaction of Au/C Core−Shell Nanostructures: In Situ Observation in the Transmission Electron Microscope. *Nano Lett* **2005**, *5*, 2092-2096.

34. Li, D.; Nielsen, M. H.; Lee, J. R. I.; Frandsen, C.; Banfield, J. F.; De Yoreo, J. J. Direction-Specific Interactions Control Crystal Growth by Oriented Attachment. *Science* **2012**, *336*, 1014-1018.
35. Wei, X.; Mulvaney, P., Optical Properties of Strongly Coupled Plasmonic Nanoparticle Clusters. In *Handbook of Surface Science*, Elsevier: 2014; Vol. 4, pp 75-108.
36. Kim, S.; Jin, J.; Kim, Y.-J.; Park, I.-Y.; Kim, Y.; Kim, S.-W. High-Harmonic Generation by Resonant Plasmon Field Enhancement. *Nature* **2008**, *453*, 757.
37. Johnson, P. B.; Christy, R.-W. Optical Constants of the Noble Metals. *Phys. Rev. B* **1972**, *6*, 4370.